



**Sulfur-Fused Perylene Diimide Electron Transport Layers
Allow >400 hr Operational Lifetime of Methylammonium
Lead Iodide Photovoltaics**

Journal:	<i>Journal of Materials Chemistry C</i>
Manuscript ID	TC-ART-07-2019-003877.R1
Article Type:	Paper
Date Submitted by the Author:	13-Aug-2019
Complete List of Authors:	Nakayama, Hidenori; Mitsubishi Chemical Corporation Zheng, Yonghao; University of Electronic Science and Technology of China, Schneider, Julia; Fordham University, Chemistry Wang, Hengbin; Mitsubishi Chemical Center for Advanced Materials, University of California Santa Barbara Ninomiya, Naoya ; Mitsubishi Chemical Corporation Yokohama Research and Development Center Momose, Tatsuya; Mitsubishi Chemical Corporation Yokohama Research and Development Center Read de Alaniz, Javier; University of California Santa Barbara, Chemistry and Biochemistry Wudl, Fred; UCSB, Department of Chemistry and Biochemistry 9510 Chabinyk, Michael; University of California Santa Barbara, Materials Department; Materials Department

Sulfur-Fused Perylene Diimide Electron Transport Layers Allow >400 hr Operational Lifetime of Methylammonium Lead Iodide Photovoltaics

Hidenori Nakayama,^{1,2} Yonghao Zheng,^{2,3} Julia A. Schneider,^{2,4,5} Hengbin Wang,² Naoya Ninomiya,¹ Tatsuya Momose,¹ Javier Read de Alaniz,^{2,4} Fred Wudl,^{2,4,6} Michael L. Chabinyc^{2,6,*}

1. Electronics Materials and New Energy Laboratory, Mitsubishi Chemical Corporation, Yokohama R&D Center 1000, Kamoshida-cho, Aoba-ku, Yokohama 227-8502, Japan

2. Mitsubishi Chemical Center for Advanced Materials, University of California, Santa Barbara, California 93106, USA

3. School of Optoelectronic Science and Engineering, University of Electronic Science and Technology of China (UESTC), Chengdu 610054, P. R. China

4. Department of Chemistry & Biochemistry, University of California, Santa Barbara, CA 93106-5050

5. Department of Chemistry, Fordham University, Bronx, USA

6. Materials Department, University of California, Santa Barbara, California 93106, USA

Abstract

Hybrid organic inorganic perovskite (HOIP) semiconductors can be used to fabricate thin film solar cells with high solar power conversion efficiencies. The stability of HOIP solar cells depends strongly on the hole and electron transport layers that encapsulate the semiconductor and prevent reactions with metallic electrodes. A series of fused perylene diimide-based compounds with varying degrees of sulfur annulation (**2PDI**, **2PDI-2S**, **2PDI-3S**, and **2PDI-4S**) were examined as electron transport layers in methyl ammonium lead iodide (MAPbI₃) solar cells. The sulfur annulation alters not only the electron affinity of the ETL, but also the chemical interaction with the MAPbI₃ layer, resulting in unusually long lifetimes for this class of devices. Devices with **2PDI-4S**, which contain two disulfide bridges, as an ETL show little degradation of the power conversion efficiency after 400 hours during solar illumination at the maximum power point, thus exceeding the performance of fullerene ETLs under long time operation.

Introduction

The last decade has witnessed an appreciable improvement in the performance of hybrid organic-inorganic perovskite photovoltaics (HOIP PVs),¹ which now reach power conversion efficiencies (PCEs) of 24% in lab-scale cells² and 19% in mini-modules.³ HOIPs comprise of materials with an ABX_3 structure, where A is a cation, B is a divalent metal and X is a halide. Efficient solar cells have been formed from methyl ammonium lead iodide ($MAPbI_3$) and structurally similar alloys with varying cations on the A site, such as cesium or formamidinium, and/or halides such as bromide.³ HOIPs can be grown from solution at low temperatures (<200 °C) via conventional coating processes, such as blade or slot-die coating, on both solid and flexible substrates.⁴ The development of complementary solution-processable materials for transport layers and encapsulation is important for improving the performance and lifetime of HOIP solar cells.

We report a study here of organic acceptors for electron transport layers (ETLs) for HOIP solar cells. These acceptors are a series of PDI dimers with a varying number of annulated sulfur atoms named **2PDI-nS** ($n = 2, 3, 4$) (Figure 1a).⁵ The number of fused sulfurs bridging the bay positions of the PDI cores tunes the EA of the compounds resulting in compounds with varying EAs (3.7, 3.9, and 4.0 eV for **2PDI-2S**, **2PDI-3S**, and **2PDI-4S**, respectively) and a deep IE (~ 5.9 eV) (Figure 1b). The comparable molecular structure, but varying degree of sulfur-atom substitution, allowed us to reveal the benefit of disulfide substitution in organic ETLs on the long-term operational stability of inverted solar cells of methyl ammonium lead iodide ($MAPbI_3$).

The typical device structure of an HOIP PV has hole and electron transport layers (HTLs and ETLs) that sandwich the HOIP layer in a *p-i-n* heterostructure.⁶ Here *p* and *n* refer to the dominant carrier type and do not necessarily mean that the HTL and ETL are intentionally doped. The design of the HTL and ETL is important to allow selective extraction of holes, or electrons, to the electrodes while also minimizing surface recombination to reduce energetic losses in the solar cell.⁷⁻⁹ The choice of ETL and HTL is also affected by the solar cell fabrication process, i.e. whether or not the material can be cast onto the chemically fragile HOIP layer. Many reports of efficient HOIP PVs have used organic materials as the HTL because these are easy to solution-process and can be tuned to line-up energetically to different HOIP materials. Inorganic oxides, such as TiO_2 , have been widely used as ETLs where they are cast prior to the HOIP layer, but can

necessitate high curing temperatures ($\sim 500\text{ }^{\circ}\text{C}$) from solution-based precursors.^{2,10,11} Such high temperatures, however, are not compatible with polymer based flexible substrates (i.e. PET and PEN) and some materials for transparent electrodes (i.e. indium tin oxide, ITO), thereby restricting its applicability and limiting possible device structures. In addition, metal oxide ETLs can be challenging to deposit onto some HOIP layers because of degradation that can occur during curing of the oxide layer at temperatures above the decomposition point of the HOIP.^{12,13}

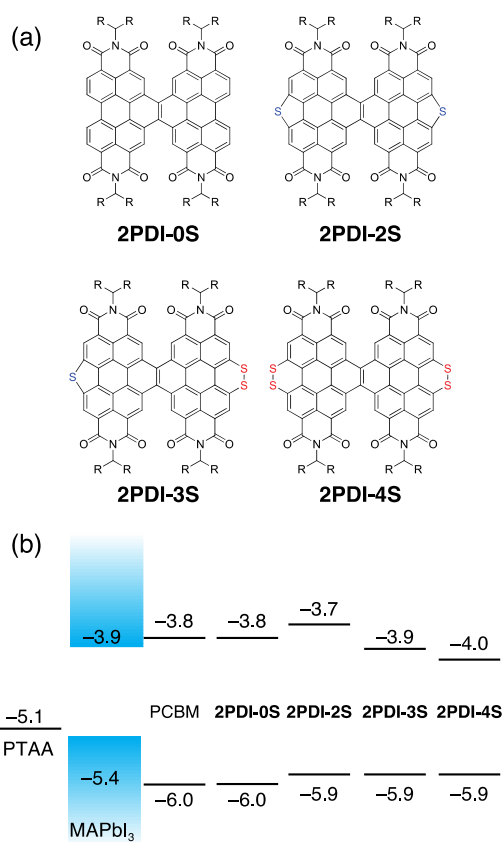


Figure 1. (a) Chemical structure of **2PDI-nS** where $R = -(\text{CH}_2)_4\text{CH}_3$. (b) Ionization energy and electron affinity of the materials used for solar cells.

Soluble organic semiconductors are promising materials for ETLs in HOIP PVs. Many organic semiconductors designed for *n*-type charge transport, or as acceptors in organic photovoltaics,^{14,15} already have the desired characteristics for HOIP ETLs. Organic ETLs that have proven successful in HOIP PVs typically have electron affinities (EAs) between 3.6 and 4.2 eV, a good match for efficient extraction of electrons from MAPbI₃ and its alloys, whose conduction band lies near 3.9

eV with respect to vacuum.^{16,17} Organic semiconductors also have ionization energies (IEs) that are deep enough to block holes (> 5.5 eV) and electron mobilities ($> 10^{-4}$ cm²/Vs) that can be improved with *n*-dopants.¹⁸ Among them, fullerene derivatives, especially phenyl-C₆₁-butyric acid methyl ester (PCBM),^{19–22} naphthalene-based polymers such as (P(NDIOD-T2)),²³ and perylene diimide (PDI) derivatives^{24–27} have been studied as ETLs with or without *n*-type dopants. These organic ETLs are usually cast onto the HOIP layer and the resulting device structure is referred to as inverted with respect to a device whose ETL was cast before the HOIP layer.

A significant question for organic ETLs is whether they can lead to devices with long lifetimes required for practical solar cells. The initial PCE of planar *p-i-n* MAPbI₃ devices with organic PCBM ETLs is ~18%, yet these have been reported to have poor stability under air exposure and light soaking, likely due to oxygen or water absorption leading to reductions in PCE by nearly a factor of 2 over ~100 hrs of testing.^{28,29} Ethylhexyl-substituted PDI ETLs in inverted structure HOIP-PVs have been reported to be relatively stable when tested by light-soaking and dark storage compared to PCBM.²⁷ They observed less decomposition of MAPbI₃ into PbI₂ and less generation of AgI at the top Ag electrode, and thus concluded that suppression of diffusion of methylammonium iodide through the PDI layer played a critical role in increasing the stability of the device. The addition of 2,9-dimethyl-4,7-diphenyl-1,10-phenanthroline (BCP) as an additional layer between fullerene ETLs, such as PCBM and C₆₀, and the metal electrode has helped to reduce degradation from contact of the metal and HOIP layer.³⁰ Overall these results suggest that it is possible to improve the lifetimes of solar cells with organic ETLs, but molecular design rules that lead to stability are still lacking.

To study the role of molecular structure on the performance of inverted MAPbI₃ PVs, we examine a series of twisted core di-PDI acceptors with varying sulfur annulation, **2PDI-nS** (*n* = 0, 2, 3, 4). Due to the twisted core of the fused PDI dimers, the compounds all form glassy or weakly ordered films by spin-coating providing comparable morphologies, yet having varying electronic levels.⁵ These compounds were shown to be effective non-fullerene acceptors in bulk heterojunction solar cells. The charge carrier mobility, based on field effect transistor measurements and time-resolved microwave conductivity, for the **2PDI-4S** was comparable to PCBM suggesting that it could act as an effective ETL for HOIP PVs.⁵ Here we compare the performance of the **2PDI-nS** series to PCBM and find that the addition of disulfide groups extends the lifetime of the solar cells under operational testing.

Results and Discussion

Performance of Solar Cells with 2PDI-nS ETLs. To study the properties of the **2PDI-nS** series as ETLs, we examined planar MAPbI₃ solar cells with an inverted structure. The materials used in the device are glass/ITO/polytriarylamine (PTAA, ~5 nm, Aldrich)/MAPbI₃ (~400 nm)/ETL/polyethyleneimine (PEIE, 80% ethoxylated, Aldrich)/Ag (80 nm) (Figure 2a). PTAA was chosen for the HTL because it has an IE of -5.1 eV and it induces relatively large grains in the MAPbI₃ active layer due to its hydrophobicity.³¹ All four **2PDI-nS** materials form uniform films on MAPbI₃ based on atomic force microscopy (Figure S1). A PEIE layer was used to improve the electric contact between the ETL and the top electrode; PEIE reduces the work function of Ag from ca. 4.7 eV³² to 3.8 eV and may also donate electrons from its amino groups to the surface of ETL^{33,34} All of the fabrication processes and measurements were conducted under a nitrogen atmosphere.

The **2PDI-nS** ETLs behaved similarly to PCBM with MAPbI₃ in as-deposited cells, but have significant differences upon thermal annealing. The **2PDI-nS** devices all show a boost in PCE upon thermal annealing at 100°C for 10 min. due to increases in fill factor (FF) and short-circuit currents (J_{SC}) up to ~20 mA/cm² (Figure 2, S2, and S3, Table 1; the statistical variation in the parameters are shown in Figures 2d, 2e, S4 and S5) The PCE increases by 50%, 90%, 42%, and 4% for **2PDI-nS**, where n = 0–4, respectively. In contrast, PCBM-containing devices exhibit decreases in both FF and J_{SC} leading to an overall 30% drop in PCE under identical annealing conditions (Figure 2a, 2b, Table 1). The incident photon-to-current efficiency (IPCE) spectra of the devices with the **2PDI-nS** ETLs (Figure 2c) are all almost identical except for the variation in magnitude. The calculated J_{SC} based on the IPCE data are 18.4, 20.7, 19.1, 20.4, 21.5 mA/cm² for PCBM, **2PDI-0S**, **2PDI-2S**, **2PDI-3S**, **2PDI-4S**, respectively, which agree with those obtained from the $J-V$ characteristics under 1 sun illumination. Overall, the **2PDI-nS** compounds benefit from the annealing process which can be attributed to improved carrier transport and extraction and thus leading to higher J_{SC} and FFs.

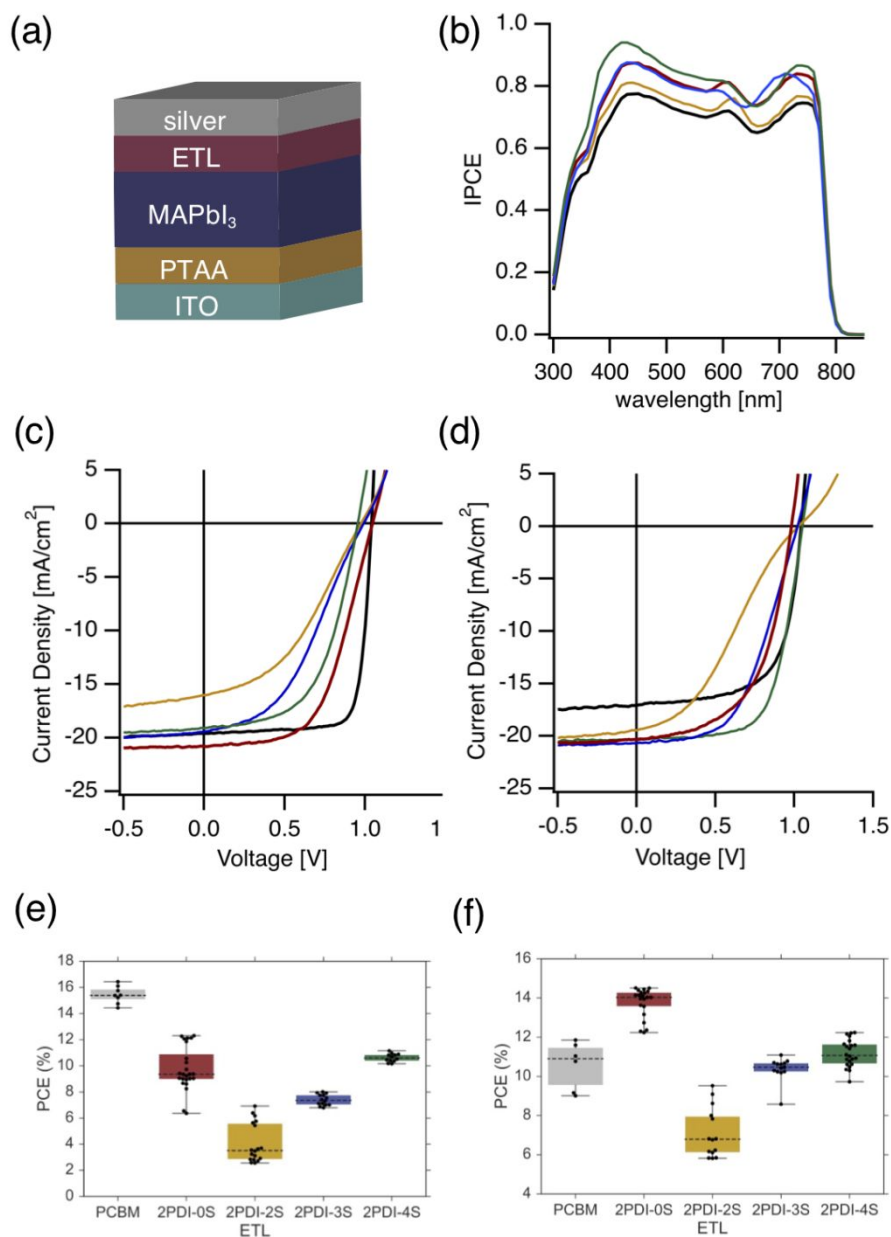


Figure 2. (a) Device structure of the MAPbI₃ solar cells. (b) Representative IPCE spectra of 100 °C 10 min annealed devices. Representative $J-V$ characteristics of the devices (c) before and (d) after 100 °C, 10 min thermal annealing. Distribution of PCEs of devices (e) before and (f) after 100 °C 10 min annealing. Five horizontal lines in each box plot represent 0, 25, 50, 75, and 100 percentile. Color coding: Black: PCBM, Red: 2PDI-0S, Gold: 2PDI-2S, Blue: 2PDI-3S, Green: 2PDI-4S.

Table 1. Device performance characteristics (median values) of MAPbI₃ solar cells with ETLs of PCBM, **2PDI-0S**, **2PDI-2S**, **2PDI-3S**, and **2PDI-4S** along with the J_{SC} calculated from the IPCE spectra. The variation of the device characteristics is shown in Figure 2.

	Device treatment	J_{SC} (mA/cm ²)	V_{OC} (V)	FF	PCE (%)	J_{SC} from IPCE (mA/cm ²)
PCBM	Pristine	19.01	1.03	0.79	15.4	-
	Annealed*	16.11	1.04	0.65	10.91	18.4
2PDI-0S	Pristine	18.43	1.02	0.49	9.36	-
	Annealed*	20.26	1.05	0.66	14.03	20.7
2PDI-2S	Pristine	13.6	0.99	0.27	3.5	-
	Annealed*	18.01	1.01	0.36	6.78	19.1
2PDI-3S	Pristine	18.37	0.99	0.41	7.36	-
	Annealed*	20.76	1.01	0.5	10.47	20.4
2PDI-4S	Pristine	19.04	0.96	0.58	10.6	-
	Annealed*	19.99	0.98	0.57	11.07	21.5

*100 °C for 10 min in nitrogen

The difference in performance of the **2PDI-nS** ETLs is more strongly related to the electron mobility of the materials rather than the EA. The J - V characteristics of the devices without PEIE layer for the **2PDI-nS** series, as well as PCBM, show a significant S-kink around the V_{OC} (Figure S6 and S7). The addition of PEIE eliminates the S-kink either by doping the ETL or significantly modifying the energetic line-up with the Ag electrode through interfacial dipoles. In both cases the differences in the V_{oc} of the devices is less than 0.1 V which is significantly smaller than the difference in the EAs of the acceptors (~ 0.3 eV). The trend in FF as a function of sulfur substitution does follow the reported trend in electron mobility for the series with **2PDI-4S** having the highest mobility. The PVs with **2PDI-4S** as an ETL, however, still underperform those with PCBM despite the material having a comparable electron mobility to PCBM.⁵

The performance of the solar cells provide insight into the interfacial contact between the **2PDI-nS** and MAPbI₃. Some organic semiconductors are known to passivate the defects at the HOIP surface by Lewis acid/base chemistry³⁵⁻³⁷ or by supplying relevant halogen ions to the vacancy sites,^{38,39} resulting in an increase in photoluminescence lifetime (decrease of recombination), diminishing the notorious hysteresis in the J - V characteristics and increasing the PCE. PCBM, for example, has been suggested to behave as a Lewis acid that accepts excess negative charges at the Pb-I antisite.³⁶ In all our **2PDI-nS** devices, we do not see notable hysteresis⁴⁰ in the J - V characteristics (Figure S2 and S3), showing that the compounds are passivating the surface of MAPbI₃. To further elucidate the response of the devices, transient photocurrents (TPCs) were measured at the short-circuit condition (Figure S8). All of the photo-currents show rapid (< 1 s) response upon turning the 1 sun illumination on or off with no obvious long time-scale ionic or capacitive contribution. The traces also show no immediate degradation in these devices with a stable current during ~ 95 s of continuous light illumination.

Interfacial Charge Transfer with the 2PDI-nS ETLs. We obtained time-resolved photoluminescence (TRPL) to further examine the role of the EA of the ETL at the interface with MAPbI₃. TRPL was collected with a low excitation fluence of ~ 0.05 $\mu\text{J}/\text{cm}^2$ that sets a carrier concentration where monomolecular recombination is expected to dominate the decay (Figure 3).^{25,28} The lifetime at short timescales of the neat MAPbI₃ film, obtained by fitting the decay with a double exponential model, is 11.6 ns (Table 2). When the MAPbI₃ layer is covered by PCBM,

2PDI-0S, or **2PDI-2S**, the decay lifetime is greatly reduced at short timescales to ~ 1 ns, indicating that electron transfer between the two layers is highly efficient. The bilayers with **2PDI-3S** and **2PDI-4S** show even shorter lifetimes (~ 0.5 ns) and very little change in the decay at longer timescales compared to the neat MAPbI₃ film. The overall trend is that the PL decays faster as the EA of the ETL increases, as observed for many undoped organic materials.^{7,17} The observed “jump” in decay lifetime between **2PDI-0/2S** and **2PDI-3/4S** also agrees with the slightly lower V_{oc} observed in the PVs without PEIE. We note that the quenching is a non-radiative loss pathway for the photogenerated carriers due to surface recombination--the carriers generated in MAPbI₃ are recombining at surface states in MAPbI₃ or recombining directly between the ETL and MAPbI₃.⁷ The V_{oc} of the devices here upon doping with PEIE, ~ 1 V, are lower than the V_{oc} in the best MAPbI₃ solar cells of 1.26 V⁴¹ and can be attributed in part to the surface recombination and also differences in the Pb precursors used to grow the MAPbI₃ layer (PbI₂ here vs. lead acetate Pb(CH₃COO)₂ in the cited work).^{42,43}

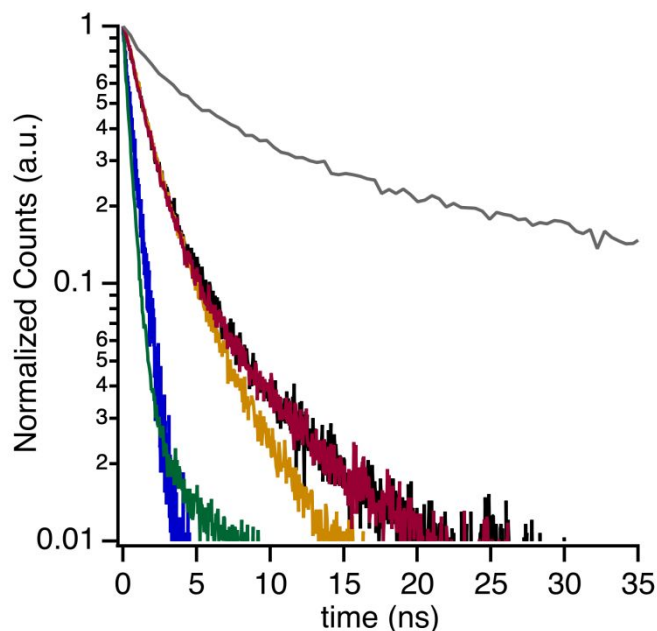


Figure 3. Time-resolved photoluminescence of MAPbI₃/ETL stacks detected at 760 nm with 400 nm excitation at 50 nJ/cm² fluence. Gray: MAPbI₃ only, Black: MAPbI₃/PCBM, Red: MAPbI₃/**2PDI-0S**, Gold: MAPbI₃/**2PDI-2S**, Blue: MAPbI₃/**2PDI-3S**, Green: MAPbI₃/**2PDI-4S**.

Table 2. Parameters from double exponential fit to the time-resolved photoluminescence curves. The general expression for the time dependence of the emission, y , yields two time constants, τ_1 and τ_2 with $y = y_0 + A_1\exp(-t/\tau_1) + A_2\exp(-t/\tau_2)$

	y_0	A_1	τ_1 (ns)	A_2	τ_2 (ns)
neat	0.0045	0.23	59.26	0.31	11.62
PCBM	0.0058	0.24	5.07	0.83	1.32
2PDI-0S	0.0037	0.17	6.11	0.90	1.39
2PDI-2S	0.0044	0.32	3.54	0.76	1.31
2PDI-3S	0.0013	0.12	1.15	0.81	0.67
2PDI-4S	0.0017	0.03	6.63	0.91	0.48

2PDI-nS ETLs Lead to MAPbI₃ Solar Cells with Long Operational Lifetimes. A surprising feature of the use of **2PDI-nS** as an ETL is the dramatic improvement in lifetimes of the solar cells compared to PCBM. We examined the stability of solar cells with the two best-performing ETLs using under continuous 1 sun illumination at 35 °C. During the illumination, the cells were connected to a resistor of 220 Ω to keep the cells operated at the maximum power. The lifetime test was started in a couple of days after the device fabrication were completed and encapsulated in nitrogen. We set time zero within 10 min after the devices were placed in the light soaking chamber. These lifetime tests showed that as-deposited **2PDI-0S** and **2PDI-4S**-based devices are significantly more stable than ones using PCBM (Figure 4 and S9). The PCBM-based device has a higher initial PCE of 17%, but shows a rapid and monotonic degradation to 2% PCE within 300 hr driven by a large decrease in J_{sc} . The operational lifetime is consistent with the values from literatures on MAPbI₃/PCBM/Ag devices (Table S1).^{27,44–47} In contrast, **2PDI-0S** and **2PDI-4S**-based devices show an increase in PCE to ~14% in the first 30 hr. This behavior differs from observations of a fast burn-in followed by a slower decay observed in some HOIP PVs. The increase in PCE is likely due to the same mechanism as that afforded by thermal annealing because both are mainly driven by the improvement of the FF . The PCE of the **2PDI-0S** device then gradually falls mainly due to decrease in the FF , while that of the **2PDI-4S** device shows a gradual increase before it plateaus after ~100 hrs and remains nearly constant until the end of the experiment at 400 hours. This increase in FF compensates for the slow decrease in J_{sc} (Figure 4). While it is difficult to compare long term stability across reports in literature because many only report shelf-life stability, the operational stability of the devices with **2PDI-4S** are comparable to best devices in literature that incorporate both metal oxide layers and an organic ETL (Table 3).

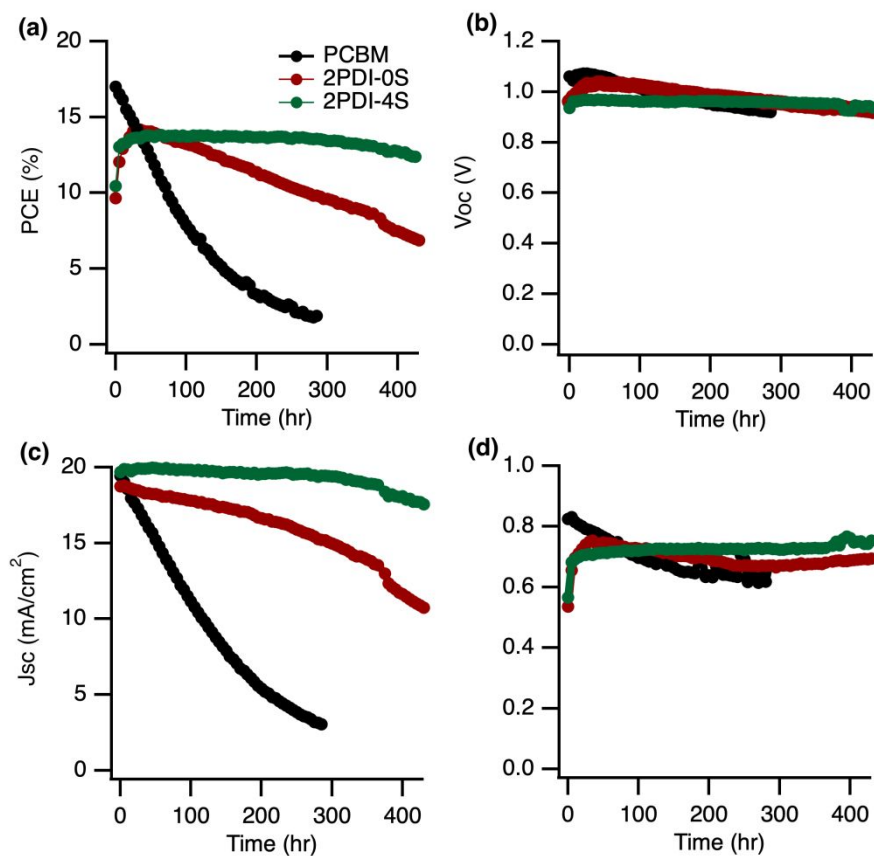


Figure 4. Device parameters of the glass cap encapsulated devices with active area of 0.16 cm² at 35 °C under continuous 1 sun illumination as a function of time. (a) PCE, (b) V_{oc} , (c) J_{sc} , and (d) FF . The devices were not annealed before illumination and the loading for the circuit was fixed to the maximum power point under 1 sun illumination before the test.

Table 3. Comparison of stability of planar inverted MAPbI₃ photovoltaics under operation

Device structure	Stabilization	Initial PCE	PCE after LS	Light Source	Atm.	Temp.	Circuit Loading	Ref
FTO/PEDOT:PSS/p-TPD/perovskite/PCBM/BCP/Au	none	15%	~0% @ 20 hr	AM 1.5G	N ₂	NA	NA	44
ITO/PEDOT:PSS/perovskite/PCBM/Ag	none	9%	<1% @ 30 hr	metal-halogen (a)	N ₂	60–70 °C	NA	27
FTO/NiMgLiO/perovskite/PCBM/Ag	none	15%	~6% @ 200 hr	White LED (b, c)	N ₂	room temperature	MPP	45
FTO/NiMgLiO/perovskite/PCBM/BCP/Ag	none	17.5%	~7% @ 600 hr	White LED (b, c)	N ₂	NA	MPP	46
ITO/PEDOT:PSS/perovskite/PDI-EH/Ag	NFA ETL	9%	~7% @ 120 hr	White Light (a)	N ₂	60–70 °C	NA	27
ITO/PTAA/perovskite/PCBM/BCP/Ag	none	15%	~10% @ 100 hr	Xenon (b)	N ₂ (d)	45–50 °C	SC	47
ITO/PTAA/perovskite/2PDI-4S/PEIE/Ag	NFA ETL	10%	~13% @ 400 hr	Xenon (b)	N₂ (d)	35 °C	MPP (e)	This Work
FTO/NiMgLiO/perovskite/PCBM/Ti(Nb)Ox/Ag	oxide layer	16%	~14.5% @ 1000 hr	AM1.5 (c)	N ₂	45–50 °C	SC	48
FTO/NiMgLiO/perovskite/PCBM/CeOx/Ag	oxide layer	18%	~18% @ 200 hr	White LED (b, c)	N ₂	room temperature	MPP	45
FTO/NiMgLiO/perovskite/4-DMABA/PCBM/BCP/Ag	passivation layer	20%	~18% @ 1000 hr	White LED (b, c)	N ₂	NA	MPP	46
ITO/PEDOT:PSS/perovskite/PCBM/Al:ZnO/ITO	oxide layer	12%	~13% @ 200 hr	sulfur plasma (b)	ambient	35 °C	MPP	49

NA = not available, NFA= non-fullerene acceptor, SC = short circuit, MPP = maximum power point (a) P = 70 mW cm², (b) P = 100 mW cm², (c)with UV cut filter, (d) glass capped with UV-curable adhesive, (e) set to MPP loading for the initial performance

Our results suggest a chemical pathway to the improvement in stability of MAPbI₃ solar cells using ETLs. Apart from the instability of MA in MAPbI₃, which can be addressed by substituting alternative A-site cations,⁵⁰ the main degradation mechanism of MAPbI₃/PCBM/Ag devices is known to be the corrosion of the silver electrode by iodides migrated from MAPbI₃ through the ETL as confirmed by time-of-flight secondary ion mass spectrometry.^{27,45} Improvement in lifetimes of HOIP solar cells have been achieved by incorporating additional cations and halogens to stabilize the HOIP layer (formamidinium, Cs),⁴⁴ inserting a protective metal oxide layer (Ti(Nb)O_x, CeO_x) between the ETL and the electrode,^{45,48} passivating the surface of MAPbI₃,⁴⁶ employing a non-halogen-corrosive material (ITO) as the electrode,⁴⁹ or adopting a non-fullerene organic semiconductor (NFA) as the ETL to reduce halogen migration rate (Table 3)²⁷. Our findings here indicate that switching to **2PDI** instead of PCBM increases the lifetime of MAPbI₃ solar cells and that the addition of disulfide bridges to **2PDI** yields a further improvement in the stability during light-soaking at the maximum power point. Annulating two sulfur atoms creates a disulfide bridge with electron-rich sulfur atoms directing electron density to the periphery of the PDI core. The disulfides increase the EA of **2PDI-4S** to 4.0 eV, within the electrochemical window of water⁵¹ and should help to stabilize the carriers in the ETL itself under operation. Disulfide bridges also form reversible redox states with free thiols, thereby increasing their reductive stability, which is paramount for an ETL. Reactions with the disulfides should help to prevent decomposition at the surface of the MAPbI₃ layer, or at the Ag electrode due to the ability of the sulfur atoms to complex inorganic ions. The relatively uniform coverage of MAPbI₃ by **2PDI-4S**, as shown in the AFM topographies (Figure S1), help to suppress ion migration to the silver electrode, but the increased lifetime performance of **2PDI-4S** suggest the disulfide moieties play an additional role in protecting the Ag electrodes. This is in line with the well-documented ability of thiols and disulfides to form self-assembled monolayers on gold and silver surfaces.⁴⁴⁻⁴⁷

Conclusions

In conclusion, we have fabricated inverted planar-structure MAPbI₃ based PV devices with **2PDI-nS** (n = 0, 2, 3, 4) as the ETL. The devices show no hysteresis in the *J-V* characteristics or slow delay time on photocurrent upon illumination, suggesting ideal electronic and physical contact between MAPbI₃ and the ETLs. AFM topography images show **2PDI-2S**, **2PDI-3S** and

2PDI-4S form smooth and grain-less films on MAPbI₃. The devices with **2PDI-0S** and **2PDI-4S** gave PCEs of 14.0% and 11.0%, respectively, after thermal annealing at 100 °C for 10min, which outperform PCBM-based devices (10.9 %). Light-soaking tests reveal that **2PDI-0S** and **2PDI-4S** devices have significantly higher stabilities than PCBM ones, especially **2PDI-4S** devices. The solar cells jump in performance during a burn-in period then show little change in the PCE over 400 hrs. Our results suggest that **2PDI-nS** compounds are suitable for realizing high performance and stable HOIP-PVs and that disulfide bridges may play a large role in protecting from corrosion of the Ag electrode by iodides.

Experimental

Thin Film and Solar Cell Preparation. Photovoltaic devices were prepared as following. Glass substrates covered by ITO (University Wafers) were sonicated in acetone and then isopropyl alcohol for 10 min each. The substrates were further cleaned with air-plasma under 300 mTorr. All of the processes hereafter were conducted under nitrogen. A 2 mg/mL solution of polytriarylamine (PTAA, Aldrich) in chlorobenzene (Aldrich) were spun-coat on the substrates at 6000 rpm. A MAPbI₃ precursor solution was formulated by dissolving a 1/1/1 (mol/mol/mol) mixture of methylammonium iodide (Dysol), lead iodide (Aldrich) and dimethyl sulfide (Aldrich) in anhydrous DMF (Aldrich).⁵² The DMF solution was spun-coat on the PTAA layer at 1000 rpm for 10 s then 4000 rpm for 30 s. When 8 s passed after the spin speed turned 4000 rpm, 0.2 mL of anhydrous chlorobenzene (Aldrich) was dropped on the substrate. The films were transferred on a hotplate of 100 °C immediately, and thermally annealed for 10 min. A solution for the ETL layer (30 mg/mL for PCBM in chlorobenzene, 20 mg/mL in toluene for the other compounds) were spun-coat on the MAPbI₃ layer at 1000 rpm, followed by a spin-coat of PEIE in isopropyl alcohol (0.02 wt%, diluted from 37% aqueous solution of PEIE from Aldrich) at 6000 rpm. The devices were finally capped with Ag (80 nm) by vacuum deposition. For the samples for photoluminescence studies, a MAPbI₃ layer was spun coat on a quartz substrate and the ETL layer was then spun coat on the MAPbI₃.

Measurements of Solar Cells. The J - V characteristics were measured at 1 sun illumination (AM 1.5G, 100mW/cm²) in a N₂-filled glovebox with a solar simulator equipped with a Xenon lamp (Newport), a Keithley 2602 Source Meter and a calibrated silicon reference cell. The voltage was scanned from 1.5 V to -0.5 V (reverse) then immediately back to 1.5 V (forward scan) at 0.01 V step to observe the hysteresis. Each step takes 30 ms for waiting and 16.7 ms for current measurement, resulting in a scan speed of 0.21 Vs⁻¹. The power conversion efficiency (PCE) was calculated with the following equation: $\text{PCE (\%)} = 100 \times V_{\text{OC}} \times J_{\text{SC}} \times \text{FF} / P_{\text{inc}}$ from the open circuit voltage, V_{OC} , the short circuit current, J_{SC} , the fill factor FF and the incident powder P_{inc} . The stability of encapsulated devices (filled with nitrogen) under illumination was examined at a maximum-power-point by using a fixed resistor (220 Ω) under continuous full-sun illumination at 35°C without UV cutting filter (SIGMAKOKI CO.,LTD, SCF-50S-42L). The active area of the cells is 0.16 cm². The incident photon to light efficiencies (IPCEs) were analyzed using a fully computerized measurement system consisting of a 300-W xenon lamp (Newport), a

monochromator (Newport CS130), a chopper controller (Newport), two current preamplifiers (SRS SR570), and two lock-in amplifiers (SRS SR810).

Time-Resolved Photoluminescence. Time-resolved photoluminescence measurements were performed using Time-Correlated Single Photon Counting (TCSPC) technique¹. Approximately 100 femtosecond (fs) excitation pulses with wavelength 400 nm were generated by doubling the fundamental frequency of fs Ti:Sapphire laser (Spectraphysics Tsunami) pulses in a commercial optical harmonic generator (Inrad). The laser repetition rate was reduced to 2 MHz by a home-made acousto-optical pulse picker in order to avoid saturation of the chromophore. TCSPC system is equipped with thermoelectrically-cooled single-photon counting avalanche photodiode (Micro Photon Devices) and electronics board (Becker & Hickl SPC-630) and has instrument response time about 30-40 picoseconds. Triggering signal for the TCSPC board was generated by sending a small fraction of the laser beam onto a fast (400 MHz bandwidth) Si photodiode (Thorlabs Inc.). Fluorescence signal was dispersed in Acton Research SPC-500 monochromator after passing through a pump blocking, long wavelength-pass, autofluorescence-free, interference filter (Omega Filters, ALP series). In addition to the time-resolved detector, the monochromator is equipped with a CCD camera (Roper Scientific PIXIS-400) allowing for monitoring of the time-averaged fluorescence spectrum. Luminescence transients were not deconvolved with the instrument response function since their characteristic time-constants were much longer than the width of the system response to the excitation pulse.

Supporting Information

Atomic force microscopy, solar cell characteristics

Author Information

Corresponding Authors

Email: mchabinyc@engineering.ucsb.edu (MLC)

Acknowledgements

The research on fundamental physical characterization of perovskite interfaces was funded by the Department of Energy Basic Energy Science Award No. DE-SC-0012541. The authors made use of the shared facilities of the UCSB MRSEC (NSF DMR 1720256), a member of the Materials Research Facilities Network. Access to Advanced Light Source at Lawrence Berkeley Laboratory was supported by the U.S. Department of Energy, Office of Science, Basic Energy Sciences under Award No. DESC-0012541.

References

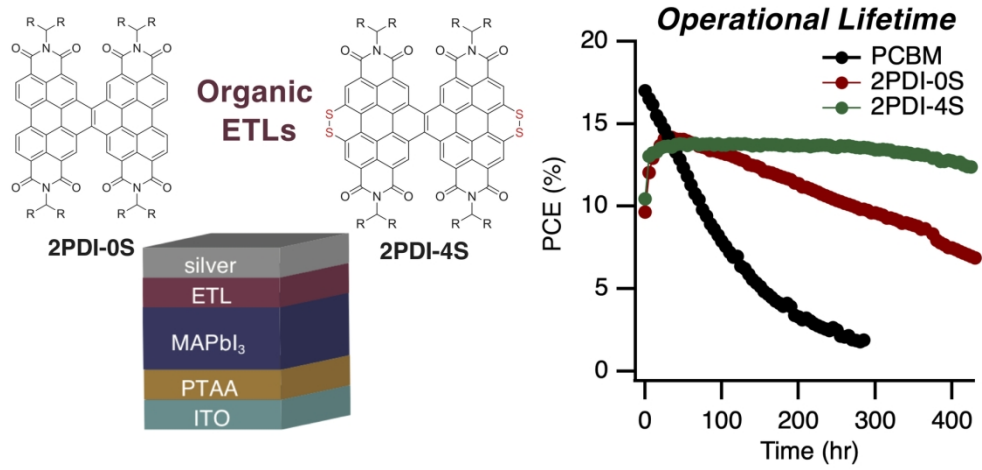
- 1 T. Miyasaka, *Chem Lett*, 2015, **44**, 720–729.
- 2 M. A. Green, E. D. Dunlop, D. H. Levi, J. Hohl-Ebinger, M. Yoshita, A. W. Y. Ho-Baillie, *Prog. Photovolt. Res. Appl.*, 2019, **27**, 565-575.
- 3 W. Li, Z. Wang, F. Deschler, S. Gao, R. H. Friend and A. K. Cheetham, *Nat Rev Mater*, 2017, **2**, 16099.
- 4 N. Park, M. Grätzel, T. Miyasaka, K. Zhu and K. Emery, *Nat Energy*, 2016, **1**, 16152.
- 5 X. Li, H. Wang, H. Nakayama, Z. Wei, J. A. Schneider, K. Clark, W.-Y. Lai, W. Huang, J. G. Labram, J. de Alaniz, M. L. Chabinye, F. Wudl and Y. Zheng, *ACS Appl. Energy Mater*, 2019, **2**, 3805-3814
- 6 A. Jena, A. Kulkarni and T. Miyasaka, *Chem Rev*, 2019, **119**, 3036-3103.
- 7 J. Wang, W. Fu, S. Jariwala, I. Sinha, A. K. Jen and D. S. Ginger, *ACS Energy Lett*, 2019, **4**, 222-227.
- 8 K. Wong, A. Fakharuddin, P. Ehrenreich, T. Deckert, M. Abdi-Jalebi, R. H. Friend and L. Schmidt-Mende, *J Phys Chem C*, 2018, **20**, 10691-10698.
- 9 B. Dänekamp, N. Droseros, D. Tsokkou, V. Brehm, P. P. Boix, M. Sessolo, N. Banerji and H. J. Bolink, *J Mater Chem C*, 2018, **7**, 523–527.
- 10 F. Giordano, A. Abate, B. JPC, M. Saliba, T. Matsui, S. Im, Zakeeruddin, M. Nazeeruddin, A. Hagfeldt and M. Graetzel, *Nat Commun*, 2016, **7**, 10379.
- 11 G. Yang, H. Tao, P. Qin, W. Ke and G. Fang, *Journal of Materials Chemistry A*, 2016, **4**, 3970–3990.

- 12 M. A. Haque, A. D. Seikh, X. Guan, T. Wu *Adv. Ener. Mater.* 2017, **7**, 1602803
- 13 E. J. Juarez-Perez, L. K. Ono, M. Maeda, Y. Jiang, Z. Hawash and Y. Qi, *J Mater Chem A*, 2018, **6**, 9604–9612.
- 14 C. Yan, S. Barlow, Z. Wang, H. Yan, A. Jen, S. R. Marder and X. Zhan, *Nat Rev Mater*, 2018, **3**, 18003.
- 15 J. Hou, O. Inganäs, R. H. Friend and F. Gao, *Nat Mater*, 2018, **17**, 119-128.
- 16 A. Said, J. Xie and Q. Zhang, *Small*, 2019, **15**, 1900854.
- 17 S. Wang, T. Sakurai, W. Wen and Y. Qi, *Adv Mater Interfaces*, 2018, **5**, 1800260.
- 18 J. T. Quinn, J. Zhu, X. Li, J. Wang and Y. Li, *J Mater Chem C*, 2017, **5**, 8654–8681.
- 19 J. Lee, J. Kim, C. Lee, G. Kim, T. Kim, H. Back, S. Jung, K. Yu, S. Hong, S. Lee, S. Kim, S. Jeong, H. Kang and K. Lee, *Adv Energy Mater*, 2017, **7**, 1700226.
- 20 Z. Wang, D. McMeekin, N. Sakai, S. Reenen, K. Wojciechowski, J. Patel, Johnston and H. Snaith, *Adv Mater*, 2017, **29**, 1604286.
- 21 J. Heo, H. Han, D. Kim, T. Ahn and S. Im, *Energy Environ Sci*, 2015, **8**, 1602–1608.
- 22 J. You, Y. Y(, Z. Hong, T. Song, L. Meng, Y. Liu, C. Jiang, H. Zhou, W. Chang, G. Li and Y. Yang, *Appl Phys Lett*, 2014, **105**, 183902.
- 23 Y. Guo, W. Sato, K. Inoue, W. Zhang, G. Yu and E. Nakamura, *J Mater Chem*, 2016, **4**, 18852–18856.
- 24 J. Huang, Z. Gu, L. Zuo, T. Ye and H. Chen, *Sol Energy*, 2016, **133**, 331–338.

- 25 S. Kim, S. Bae and W. Jo, *RSC Advances*, 2016, **6**, 19923–19927.
- 26 H. Zhang, L. Xue, J. Han, Y. Fu, Y. Shen, Z. Zhang, Y. Li and M. Wang, *J Mater Chem*, 2016, **4**, 8724–8733.
- 27 A. Akbulatov, L. Frolova, M. Griffin, I. Gearba, A. Dolocan, D. Bout, S. Tsarev, E. Katz, A. Shestakov, K. Stevenson and P. Troshin, *Adv. Ener. Mater.*, 2017, 1700476.
- 28 J. You, L. Meng, T.-B. Song, T.-F. Guo, Y. Yang, W.-H. Chang, Z. Hong, H. Chen, H. Zhou, Q. Chen, Y. Liu, N. Marco and Y. Yang, *Nat Nanotechnol*, 2015, **11**, 75–81.
- 29 L. Meng, J. You, T.-F. Guo and Y. Yang, *Acc. Chem Res*, 2016, **49**, 155–165.
- 30 D. Liu, Q. Wang, C. J. Traverse, C. Yang, M. Young, P. S. Kuttipillai, S. Y. Lunt, T. W. Hamann and R. R. Lunt, *ACS Nano*, 2017, **12**, 876–883.
- 31 C. Bi, Q. Wang, Y. Shao, Y. Yuan, Z. Xiao and J. Huang, *Nat Commun*, 2015, **6**, 7747.
- 32 Y. Zhou, C. Fuentes-Hernandez, J. Shim, J. Meyer, A. Giordano, H. Li, P. Winget, T. Papadopoulos, H. Cheun, J. Kim, M. Fenoll, A. Dindar, W. Haske, E. Najafabadi, T. Khan, H. Sojoudi, S. Barlow, S. Graham, J. Brédas, S. Marder, A. Kahn and B. Kippelen, *Science*, 2012, **336**, 327–332.
- 33 C. Li, C. Chueh, F. Ding, H. Yip, P. Liang, X. Li and A. Jen, *Adv. Mater.*, 2013, **25**, 4425–4430.
- 34 B. Russ, M. Robb, B. Popere, E. Perry, C. Mai, S. Fronk, S. Patel, T. Mates, G. Bazan, J. Urban, M. Chabynyc, C. Hawker and R. Segalman, *Chem. Sci.*, 2015, **7**, 1914–1919.
- 35 D. deQuilettes, S. Koch, S. Burke, R. Paranjji, A. Shropshire, M. Ziffer and D. Ginger, *ACS Energy Lett*, 2016, **1**, 438–444.

- 36 J. Xu, A. Buin, A. Ip, W. Li, O. Voznyy, R. Comin, M. Yuan, S. Jeon, Z. Ning, J. well, P. Kanjanaboos, J. Sun, X. Lan, L. Quan, D. Kim, I. Hill, P. Maksymovych and E. Sargent, *Nature Comm.*, 2015, **6**, 7081.
- 37 N. Noel, A. Abate, S. Stranks, E. Parrott, V. Burlakov, A. Goriely and H. Snaith, *ACS Nano*, 2014, **8**, 9815–9821.
- 38 X. Zheng, B. Chen, J. Dai, Y. Fang, Y. Bai, Y. Lin, H. Wei, X. Zeng and J. Huang, *Nature Energy*, 2017, **2**, 17102.
- 39 N. Aristidou, C. Eames, I. Sanchez-Molina, X. Bu, J. Kosco, Islam and S. Haque, *Nat Commun*, 2017, **8**, 15218.
- 40 S. N. Habisreutinger, N. K. Noel and H. J. Snaith, *ACS Energy Lett*, 2018, **3**, 2472–2476.
- 41 Z. Liu, L. Krückemeier, B. Krogmeier, B. Klingebiel, J. A. Márquez, S. Levchenko, S. Öz, S. Mathur, U. Rau, T. Unold and T. Kirchartz, *ACS Energy Lett*, 2018, 110–117.
- 42 F. Aldibaja, L. Badia, E. Mas-Marzá, R. S. Sánchez, E. M. Barea and I. Mora-Sero, *J Mater Chem A*, 2014, **3**, 9194–9200.
- 43 W. Zhang, M. Saliba, D. T. Moore, S. K. Pathak, M. T. Hörantner, T. Stergiopoulos, S. D. Stranks, G. E. Eperon, J. A. Alexander-Webber, A. Abate, A. Sadhanala, S. Yao, Y. Chen, R. H. Friend, L. A. Estroff, U. Wiesner and H. J. Snaith, *Nat Commun*, 2015, **6**, 6142.
- 44 M. Alsari, A. J. Pearson, J. Wang, Z. Wang, A. Montisci, N. C. Greenham, H. J. Snaith, S. Lilliu and R. H. Friend, *Sci Reports*, 2018, **8**, 5977.
- 45 R. Fang, S. Wu, W. Chen, Z. Liu, S. Zhang, R. Chen, Y. Yue, L.-L. Deng, Y. Cheng, L. Han and W. Chen, *ACS Nano*, 2018, **12**, 2403–2414.

- 46 H. Zhu, B. Huang, S. Wu, Z. Xiong, J. Li and W. Chen, *J Mater Chem A*, 2018, **6**, 6255–6264.
- 47 Z. Zhou, X. Li, M. Cai, F. Xie, Y. Wu, Z. Lan, X. Yang, Y. Qiang, A. Islam and L. Han, *Adv Energy Mater*, 2017, **7**, 1700763.
- 48 W. Chen, Y. Wu, Y. Yue, J. Liu, W. Zhang, X. Yang, H. Chen, E. Bi, I. Ashraful, M. Grätzel and L. Han, *Science*, 2015, **350**, 944–948.
- 49 K. A. Bush, C. D. Bailie, Y. Chen, A. R. Bowring, W. Wang, W. Ma, T. Leijtens, F. Moghadam and M. D. McGehee, *Adv. Mater.* , 2016, **28**, 3937–3943.
- 50 C. C. Boyd, R. Cheacharoen, T. Leijtens and M. D. McGehee, *Chem Rev*, 2019, **119**, 3418–3451.
- 51 D. M. de Leeuw, M. M. J. Simenon, A. R. Brown and R. E. F. Einerhand, *Synthetic Met*, 1997, **87**, 53–59.
52. J. Feng, X. Zhu, Z. Yang, X. Zhang, J. Niu, Z. Wang, S. Zuo, S. Pirya, S. Liu, D. Yang *Adv. Mater.* 2018, **30**, 1801418.



163x78mm (300 x 300 DPI)